

# Carbon-supported manganese oxide nanoparticles as electrocatalysts for oxygen reduction reaction (orr) in neutral solution

I. Roche · K. Scott

Received: 15 May 2008 / Accepted: 18 August 2008 / Published online: 12 September 2008  
© Springer Science+Business Media B.V. 2008

**Abstract** Manganese oxides ( $\text{MnO}_x$ ) catalysts were chemically deposited onto various high specific surface area carbons. The  $\text{MnO}_x/\text{C}$  electrocatalysts were characterised using a rotating disk electrode and found to be promising as alternative, non-platinised, catalysts for the oxygen reduction reaction (ORR) in neutral pH solution. As such they were considered suitable as cathode materials for microbial fuel cells (MFCs). Metal [Ni, Mg] ion doped  $\text{MnO}_x/\text{C}$ , exhibited greater activity towards the ORR than the un-doped  $\text{MnO}_x/\text{C}$ . Divalent metals favour oxygen bond splitting and thus orientate the ORR mechanism towards the 4-electron reduction, yielding less peroxide as an intermediate.

**Keywords** Oxygen reduction reaction · Microbial fuel cell · Manganese oxides · Neutral pH · Electrocatalysis

## 1 Introduction

Poor kinetics of the oxygen reduction reaction electrocatalysts (ORR) at neutral pH and low temperatures can hinder the performance and development of fuel cells under these conditions [1–3]. This is especially the case in, for example, microbial fuel cells (MFCs) where low power performance would necessitate high capital cost, especially for the electrodes. Platinum is known to be the best catalyst for the ORR in acid and alkaline media [4]. However, for

simple cost reasons, non-platinised materials represent a necessary alternative. There has been limited research into catalysts for the ORR in neutral solution and very few platinum free catalysts have been studied. Electrochemical studies have been carried out in neutral solution with metal tetramethoxyphenylporphyrin (TMPP), CoTMPP and FeCoTMPP, and metal phthalocyanine (Pc), FePc, CoPc and FeCuPc, supported on Ketjenblack (KJB) carbon: the FePc/KJB catalysts exhibited very good activity towards the ORR [5].

Manganese oxides are promising as catalysts for ORR in neutral media [6]. Electrochemical properties of manganese oxides have been studied in alkaline media, but very few studies have been carried out at neutral pH [7, 8]. Chartier et al. described rather good activity of  $\text{MnO}_x$  in neutral and slightly acid media, together with the role of the  $\text{Mn}^{\text{IV}}/\text{Mn}^{\text{III}}$  redox couple on the 4 and 2 electron oxygen reduction mechanisms [7, 8]. However these studies concerned mixed valency spinel  $\text{Cu}_x\text{Mn}_{3-x}\text{O}_4$  oxides. No studies, to our knowledge, have been carried out on  $\text{MnO}_x/\text{C}$ -based materials as electrocatalysts for the ORR at neutral pH.

Carbon-supported manganese oxides nanoparticles were found to exhibit good ORR activity in alkaline media [9–13]. In addition the doping of  $\text{MnO}_x/\text{C}$  by the divalent ions  $\text{Ni}^{\text{II}}$ ,  $\text{Mg}^{\text{II}}$  or  $\text{Ca}^{\text{II}}$ , was found to be extremely promising, since the Me- $\text{MnO}_x/\text{C}$  catalysts exhibited ORR activity close to that of a benchmark Pt/Vulcan XC72 from E-Tek [12, 13]. We have characterised the ORR activity of such  $\text{MnO}_x/\text{C}$ -based catalysts in neutral pH solution.

The present work has evaluated the activity of carbon-supported  $\text{MnO}_x$  electrocatalysts towards the ORR at neutral pH for use as cathode material in MFCs. In particular the influence of the doping of  $\text{MnO}_x/\text{C}$ -based electrocatalysts and the carbon support, on the ORR

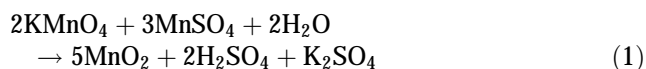
I. Roche (✉) · K. Scott  
School of Chemical Engineering and Advanced Materials,  
University of Newcastle upon Tyne, Newcastle upon Tyne NE1  
7RU, UK  
e-mail: rochivan@yahoo.fr

activity of the carbon-supported manganese oxide nanoparticles, was studied. Results were compared to those of a benchmark 20% by weight (20 wt.%) Pt/Vulcan XC72 from E-Tek. The ORR mechanism on  $\text{MnO}_x/\text{C}$ -based catalysts was also studied.

## 2 Experimental

### 2.1 Synthesis of $\text{MnO}_x/\text{C}$ materials

The manganese oxide nanoparticles were chemically deposited onto the carbon substrate as follows [10, 11]: 4 g of carbon was mixed with a 70 cm<sup>3</sup> (mL) of an aqueous solution containing 10 mmol (mM) of  $\text{MnSO}_4$  (Aldrich). The suspension was maintained at a controlled temperature (80 °C) for 20 min under magnetic stirring, in order to allow impregnation of the carbon by manganese sulphate. A 300 mL aqueous solution, containing 33 mmol of  $\text{KMnO}_4$  (Merck), previously heated at controlled 80 °C, was then gradually added to the agitated suspension.  $\text{MnSO}_4$  is oxidized by the permanganate in the presence of the carbon according to the chemical reaction [14]:



The reaction medium was maintained at 80 °C under agitation for 15 min and then washed, filtered and dried at 100 °C for approximately 10 h. The corresponding mass ratios in the obtained  $\text{MnO}_x/\text{C}$  material were 4.0 g of C to 2.4 g of Mn. The specific surface areas of Vulcan XC72 (called Vulcan) and Monarch 1000 (called Monarch), were 240 and 300 m<sup>2</sup> g<sup>-1</sup>, respectively [14]. The suspension was maintained at a controlled temperature (80 °C) for 15 min and then filtered and dried at 100 °C. Similar oxidations, using potassium permanganate, were performed on the carbon supports alone, and these are named as Vulcan XC72<sub>ox</sub> or Monarch1000<sub>ox</sub>.

To prepare the Ni, Mg or Ca-doped catalysts, a solution (0.01 mol) of  $\text{Ni}(\text{NO}_3)_2 \cdot 6\text{H}_2\text{O}$  (Aldrich),  $\text{Mg}(\text{NO}_3)_2 \cdot 6\text{H}_2\text{O}$  or  $\text{Ca}(\text{NO}_3)_2 \cdot 4\text{H}_2\text{O}$  (Aldrich) was added prior to the permanganate addition [10].

All  $\text{MnO}_x/\text{C}$ -based catalysts should exhibit a Mn loading of ca. 20 wt.%, and Me loadings of ca. 7, 3 and 4 wt.% for Me = Ni, Mg and Ca, respectively, at the time of their synthesis according to previous reports of this preparation method [10]. If all the Mn is present as  $\text{MnO}_2$ , the materials should have a  $\text{MnO}_2$  loading of ca. 30 wt.%. Previous papers [10, 13] have shown evidence that the manganese oxides are well dispersed over the carbon support as  $\text{MnO}_2$ . However, X-ray diffraction (XRD) experiments were undertaken for the  $\text{MnO}_x/\text{C}$ -based materials. Using the manganese loading values, the current densities with

respect to the mass of active materials were calculated. A more precise physico-chemical characterisation of the  $\text{MnO}_x/\text{C}$ -based materials is part of on-going work.

### 2.2 XRD characterisation

The chemistry of  $\text{MnO}_x$  particles supported on carbon black is complex. In order to determine the  $\text{MnO}_x$  crystallographic structures on the carbon, X-ray diffraction (XRD) for all our  $\text{MnO}_x/\text{C}$ -based materials was performed on a Panalytical (ex-Philips) X'Pert Pro MPD (multi purpose diffractometer) equipped with a diffracted-beam monochromator, using Cu K $\alpha$  radiation. The XRD characterisations were carried out in the *Chemical and Materials Analysis Services*, Sage Faculty, University of Newcastle (United Kingdom).

### 2.3 Materials and electrodes

Glassy carbon tips (diameter,  $\phi$  3.0 mm, 0.071 cm<sup>2</sup><sub>geom.</sub>) were used as catalyst substrates to characterise the active layers of the catalysts. As described previously [12, 13], each active layer was deposited from an ink containing 25 mg of  $\text{MnO}_x/\text{C}$  or Me- $\text{MnO}_x/\text{C}$  (Me = [Ni, Mg, Ca]) powder, 1 cm<sup>3</sup> of water, 0.6 cm<sup>3</sup> of propan-2-ol and of PTFE solution (60 wt.%, Aldrich). After homogenisation by sonication, a 0.002 cm<sup>3</sup> drop of the ink was deposited onto the glassy carbon electrode and solvents were evaporated at room temperature. The resulting porous active layer (containing ca. 14 wt.% PTFE on the basis of the dry materials) was then heat treated at 100 °C for 15 min to ensure its mechanical stability. A rotating disc electrode (Autolab, Netherlands) was used to evaluate the electrochemical activity of the  $\text{MnO}_x/\text{C}$  materials. All solutions were prepared with de-ionised water.

### 2.4 Electrochemical cells

The electrochemical tests were performed in 0.1 M  $\text{Na}_2\text{SO}_4$  solution in a three-electrode glass cell. The initial pH was measured at ca. 7. A phosphate buffer medium was not used as this would have been potentially detrimental to the  $\text{MnO}_2$  catalyst activity. A platinum foil was used as the counter electrode, the RDE as working electrode and the reference was a Ag/AgCl (sat) electrode ( $E^\circ = +0.197$  V vs. SHE). All potentials are referred to the standard hydrogen electrode (SHE). Voltammetry was conducted using a computer-controlled potentiostat (Sycopel Scientific LTD, England). "Blank" experiments under nitrogen (BOC, England) were performed to characterise the active layers in terms of their stability in the ORR potential range. ORR voltammetry was carried out after oxygen (BOC, England) saturation of the electrolyte and the oxygen

saturation concentration was maintained by O<sub>2</sub> bubbling in the solution. The solution temperature was thermostated at 25 (±1) °C. Successive ORR voltammograms were recorded on the MnO<sub>x</sub>/C-based active layers (immobilized as the porous active layer on the glassy-carbon disk) from +0.7 V to −0.5 V (vs. SHE) at quasi-steady-state conditions (1 mV s<sup>−1</sup>) for various RDE speeds of rotation. Prior to each voltammetric sweep the potential was maintained at a starting potential, +0.7 V vs. SHE, for 2 min, to ensure identical initial surface-states of all active layers.

### 3 Results and discussion

#### 3.1 XRD results

XRD spectra (Fig. 1) revealed the diagnostic interlayer reflection typical for γ-MnO<sub>2</sub> [15] for the MnO<sub>x</sub>/C-based materials for both carbon supports (Vulcan or Monarch). The XRD patterns did not reveal segregated nickel, magnesium or calcium domains, indicating that the divalent metals were inserted into the manganese oxide crystal lattice: true metal doping. The XRD peak at 2θ = 36.8° was moved to a lower angle with doping; indicating metal insertion between the manganese oxide layers (Fig. 1), in agreement with previous reports [11, 13]. A volume average diameter of ca. 10 nm of the manganese oxide nanocrystallites (L<sub>v</sub>) was estimated, starting from the XRD spectra (peaks 2θ = 36.8° and 66.2° considered) and by considering the classical Scherrer equation [16]. However, TEM images are also required to confirm the previous XRD results and to estimate the particle size distribution of the MnO<sub>2</sub> particles dispersed over the carbon support. This is part of on-going work.

#### 3.2 Proton insertion

Cyclic voltammograms obtained in N<sub>2</sub>-saturated 0.1 M Na<sub>2</sub>SO<sub>4</sub> solution (pH ca. 7), for MnO<sub>x</sub>/C materials were stable on potential cycling between the second and twentieth cycles (Fig. 2): from +1.2 to +0.6 V vs. SHE. The

material underwent reduction of metastable oxides, as revealed by the reduction peak around +0.87 V vs. SHE, corresponding to Eq. 2 [17]:



The peak potential was in agreement with that found in the Pourbaix diagram. Proton insertion (2) is followed by the 1-electron reduction of MnOOH yielding Mn<sup>2+</sup> ions. This reduction is, however, strongly limited by resistive effects due to the low conductivity of MnOOH. As a consequence, MnOOH is partially dissolved in the electrolyte.

The catalytic activity of MnO<sub>x</sub>/C materials has been shown to decrease upon potential cycling in alkaline medium; proton insertion thus being not totally reversible [12, 13]. The manganite (MnOOH) formed was quite soluble in alkaline medium and easily dissolved into the solution [18], the catalytic activity associated with the peak currents being then lost upon cycling. It has been shown that inclusion of divalent metal ions favoured stabilisation of Mn<sup>IV</sup>/Mn<sup>III</sup> species in alkaline medium, proton insertion then being reversible [13]. In contrast to experiments carried out in alkaline medium, cyclic voltammograms for MnO<sub>x</sub>/C-based catalysts at neutral pH showed very stable electrocatalytic activity even for un-doped MnO<sub>x</sub>/C catalysts, as there was little, if any, dissolution of MnOOH in neutral electrolyte. The experimental results were very

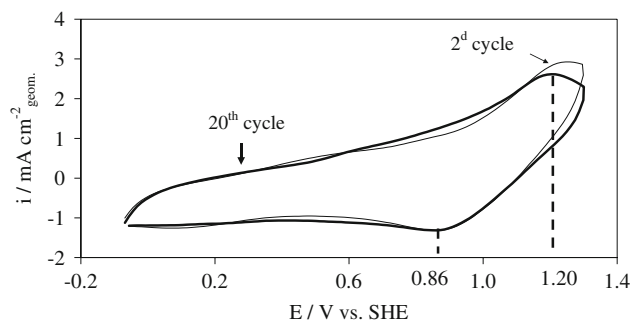
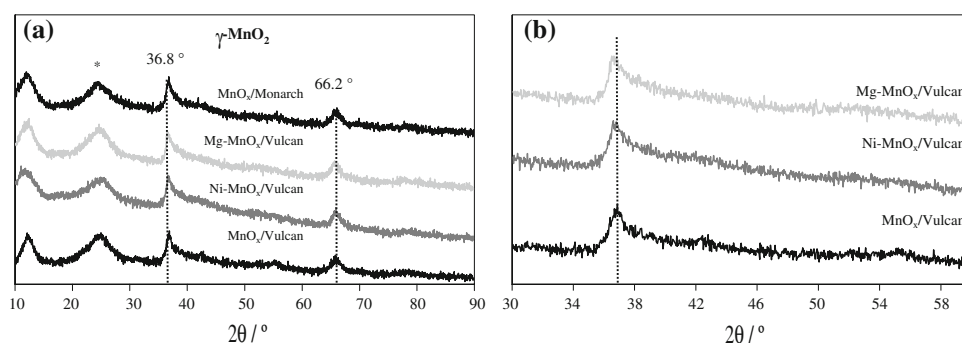


**Fig. 2** Cyclic voltammograms for the MnO<sub>x</sub>/Vulcan catalyst. 2<sup>d</sup> (black) and 20<sup>th</sup> (gray) cycles, N<sub>2</sub>-saturated 0.1 M Na<sub>2</sub>SO<sub>4</sub> solution (pH ca. 7), at 25 °C, scan rate 0.1 V s<sup>−1</sup>, speed of rotation Ω = 0

**Fig. 1** (a) XRD spectra of MnO<sub>x</sub>/Vulcan, Ni-MnO<sub>x</sub>/Vulcan, Mg-MnO<sub>x</sub>/Vulcan, and MnO<sub>x</sub>/Monarch. The γ-MnO<sub>2</sub> phase is apparent (considered peaks: 2θ = 36.8° and 66.2°. \*diffraction peak of the carbon support. (b) 2θ = 36.8° peak, considered for the MnO<sub>x</sub>/Vulcan-based materials



repeatable. This very good stability suggests there was no loss of active material in neutral pH solution.

### 3.3 ORR activity

Successive voltammograms obtained in oxygen-saturated, 0.1 M Na<sub>2</sub>SO<sub>4</sub> solution (pH ca. 7) for the MnO<sub>x</sub>/C active layers deposited on the RDE are shown in Fig. 3a, for MnO<sub>x</sub>/Monarch. Similar voltammograms were obtained for carbons (C<sub>ox</sub>), previously oxidised by permanganate, to determine the influence of the carbon support on electrochemical activity (see the example of the carbon Monarch<sub>ox</sub> at 2,500 rpm, Fig. 3a). The pure Faradaic current for the ORR was obtained after subtraction of the blank current under nitrogen obtained under the same voltammetry conditions at which proton insertion occurs. The electrolyte was not buffered. During proton insertion, changes in the interfacial H<sup>+</sup> concentration could consequently be in the proximity of the active layer surface, especially for such MnO<sub>x</sub>/C-based materials having a high specific surface area. In the coulombic charge regions the blank current were 10 to 20 times lower than currents under O<sub>2</sub>. The ORR currents were then not significantly affected by possible interfacial pH variations. The current densities were limited, especially at high current densities, by oxygen diffusion in the solution and in the active layer, following the equation:

$$1/|i_{\text{exp.}}| = 1/|i_k| + 1/|i_1^{\text{diff. solution}}| + 1/|i_1^{\text{diff. activelayer}}| \quad (3a)$$

$$1/|i_{\text{exp.}}| = 1/|i_k| + 1/(B\Omega^{1/2}) + 1/|i_1^{\text{diff. activelayer}}| \quad (3b)$$

where,

$$B = 0.620 n F C_{O_2} D_{O_2}^{2/3} \nu^{-1/6} \quad (4)$$

is the Levich slope,  $i_{\text{exp.}}$  is the measured current density at a given potential and revolution speed ( $\Omega/\text{rad s}^{-1}$ ) of the RDE,  $i_k$  the ORR kinetic current density,  $i_1$  the ORR limiting current density in the solution,  $n$  the number of exchanged electrons,  $F$  the Faraday constant ( $96,487 \text{ C mol}^{-1}$ ).  $D_{O_2}$  is the diffusion coefficient of O<sub>2</sub> in 0.1 M Na<sub>2</sub>SO<sub>4</sub> aqueous solution,  $\nu$  is the kinematic viscosity of the solution and  $C_{O_2}$  is the oxygen concentration in the O<sub>2</sub>-saturated solution.

Under air the oxygen solubility is  $6 \text{ mg L}^{-1}$  for seawater at 25 °C. It is then accordingly approximately  $1.9 \times 10^{-6} \text{ mol cm}^{-3}$  for O<sub>2</sub>-saturated seawater. The kinematic viscosity of the aqueous electrolyte is ca.  $0.01 \text{ cm}^2 \text{ s}^{-1}$  at 25 °C and the oxygen diffusion coefficient  $D_{O_2}$  is ca.  $1.9 \times 10^{-5} \text{ cm}^2 \text{ s}^{-1}$ . Using these values,  $B \approx 0.1 n (\text{mA cm}^{-2} \text{ rad}^{-1/2} \text{ s}^{1/2})$ .

The classical Tafel representations of the kinetic current densities in the ORR potential range for our MnO<sub>x</sub>/C-based catalysts (see the example of Monarch<sub>ox</sub>, MnO<sub>x</sub>/Monarch and Ni-MnO<sub>x</sub>/Monarch) is shown in Fig. 3b. The current

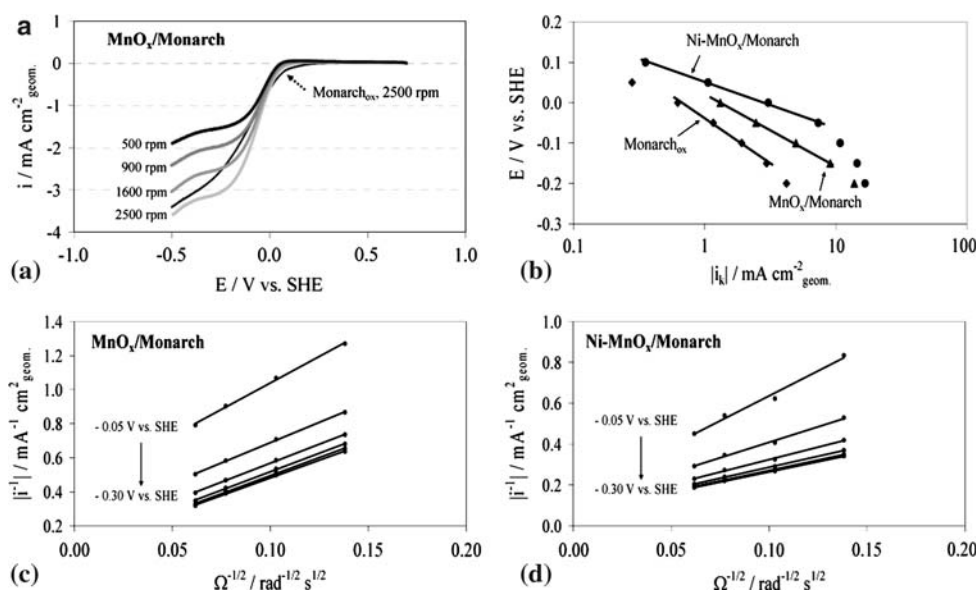


**Fig. 3** (a) Voltammograms for the MnO<sub>x</sub>/Monarch catalyst at different RDE rotation rates (500, 900, 1,600 and 2,500 rpm). Currents corrected for the blank, and for Monarch<sub>ox</sub>, previously oxidized. O<sub>2</sub>-saturated 0.1 M Na<sub>2</sub>SO<sub>4</sub> solution at 25 °C, 0.001 V s<sup>-1</sup>. (b) Corresponding Tafel plots, in the low current densities range, for Ni-MnO<sub>x</sub>/Monarch ( $b = -0.113 \text{ V dec}^{-1}$ ), MnO<sub>x</sub>/Monarch

( $b = -0.177 \text{ V dec}^{-1}$ ) and Monarch<sub>ox</sub>, previously oxidized ( $b = -0.161 \text{ V dec}^{-1}$ ). The currents were corrected for O<sub>2</sub> diffusion in the solution and in the active layer. (c) Koutecky-Levich plots for MnO<sub>x</sub>/Monarch at different potentials: -0.05, -0.10, -0.15, -0.20, -0.25 and -0.30 V vs. SHE. (d) Koutecky-Levich plots for Ni-MnO<sub>x</sub>/Monarch at the same ORR potentials

**Table 1** Kinetic parameters for the ORR in O<sub>2</sub>-saturated 0.1 M Na<sub>2</sub>SO<sub>4</sub> at 25 °C—corrected for oxygen diffusion in solution and the active layer. Potentials at current on-set, kinetic current densities at 0 V vs. SHE, corresponding mass activities (MA), based on the mass of platinum (Pt/C) or manganese dioxide (un-doped and doped)

Catalysts	E <sub>on-set</sub> /V vs. SHE	i <sub>k</sub> /mA cm <sup>-2</sup> <sub>geom.</sub>	MA/A g <sub>Pt/MnO<sub>2</sub></sub> <sup>-1</sup>	b/V dec <sup>-1</sup>
MnO <sub>x</sub> /Vulcan	+0.29	0.6	4	-0.134
Ni-MnO <sub>x</sub> /Vulcan	+0.33	1.3	9	-0.335
Mg-MnO <sub>x</sub> /Vulcan	+0.28	0.7	5	-0.305
Ca-MnO <sub>x</sub> /Vulcan	+0.18	0.2	2	-0.129
MnO <sub>x</sub> /Monarch	+0.25	1.3	9	-0.177
Ni-MnO <sub>x</sub> /Monarch	+0.26	2.8	19	-0.113
Pt/Vulcan (E-Tek)	+0.49	18.0	100	-0.213

densities were mass transfer corrected for the diffusion of oxygen in the solution, using the classical [19] Koutecky-Levich model (see Figs. 3c, d for MnO<sub>x</sub>/Monarch and Ni-MnO<sub>x</sub>/Monarch, respectively). The current densities were also corrected for the diffusion of oxygen in the active layer using the macro-homogeneous model [20]. The results of kinetic parameters obtained for doped and un-doped MnO<sub>x</sub>/C are summarized in Table 1, together with those for the benchmark 20 wt.% Pt/Vulcan XC72 (E-Tek).

Estimation of the active surface area (SA) of the MnO<sub>x</sub>/C catalysts was approximate because the manganese oxide particles size distribution was unknown. Current densities were thus referred to the geometric electrode area and the mass activities (MA) of the catalysts (Table 1). As a first approximation, all the Mn was assumed to be present as active MnO<sub>2</sub>, with a loadings of ca. 20 wt.%. [13]. Also in comparing the data for Pt and Mn/C catalyst in the case of Mn it should be noted that there was half the mass in the active layer. Physico-chemical characterisation of the MnO<sub>x</sub>/C-based materials to determine the morphology and chemistry of the manganese oxide particles dispersed on the carbon substrate is part of on-going work.

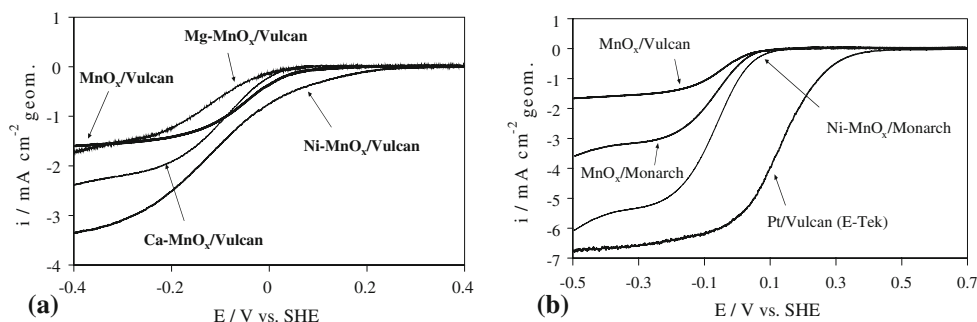
Kinetic parameters determined from the RDE studies were the Tafel slope in the low current density range, b, and the kinetic current density at 0.0 V vs. SHE (Fig. 3b). The high current density was not considered because the linear zones were poorly defined in the low ORR potential

range (E < -0.2 V vs. SHE), and the adsorption isotherms of oxygenated species were probably different on the surfaces of manganese oxides and platinum.

The oxidised carbon support showed appreciable activity in the ORR potential range (see the example of Monarch<sub>ox</sub>, Fig. 3b). The presence of oxygenated groups on the surface of the carbon, partially formed by oxidation with permanganate, may facilitate oxygen reduction, as reported by Kinoshita [4]. However, dispersion of manganese oxides onto the high area carbon substrates improved the ORR activity at neutral pH in the low current density range (Fig. 3b). The influence of the carbon substrate was more significant in the case of the carbon Monarch<sub>ox</sub>: indeed, at 0.0 V vs. SHE, the geometric ORR kinetic current densities |i<sub>k</sub>| were ca. +0.6 and +1.3 mA cm<sup>-2</sup><sub>geom.</sub>, for Monarch<sub>ox</sub> and the MnO<sub>x</sub>/Monarch catalyst, respectively (Table 1). The ORR activity of the 20 wt.% Pt/Vulcan XC72 was around 10 times higher than that of manganese oxide: MA were ca. 100 A g<sub>Pt</sub><sup>-1</sup> at 0.0 V vs. SHE compared to 9.0 A g<sub>MnO<sub>2</sub></sub><sup>-1</sup> for MnO<sub>x</sub>/Monarch (Table 1). The Pt/Vulcan XC72 catalyst exhibited a lower ORR overvoltage (ca. 0.26 V) than un-doped MnO<sub>x</sub>/C electrocatalysts (Table 1, Fig. 4).

For the MnO<sub>x</sub>/Vulcan-based catalysts, Ni<sup>II</sup> doping improved the ORR kinetics in the low current density range; the MA was 9 for Ni-MnO<sub>x</sub>/Vulcan, compared to 4 A g<sub>MnO<sub>2</sub></sub><sup>-1</sup> for un-doped MnO<sub>x</sub>/Vulcan (Table 1). Doping

**Fig. 4** (a) Linear Sweep Voltammograms for the MnO<sub>x</sub>/Vulcan-based materials. Scan rate 0.001 V s<sup>-1</sup>, 2,500 rpm, O<sub>2</sub>-saturated 0.1 M Na<sub>2</sub>SO<sub>4</sub> solution, 25 °C. (b) LSVs for MnO<sub>x</sub>/Vulcan, MnO<sub>x</sub>/Monarch, Ni-MnO<sub>x</sub>/Monarch and the 20 wt.% Pt/Vulcan XC72, 2,500 rpm, O<sub>2</sub>-saturated 0.1 M Na<sub>2</sub>SO<sub>4</sub> solution, 25 °C, scan rate 0.001 V s<sup>-1</sup>



with Mg or Ca did not improve the oxygen reduction kinetics: the ORR potential was more negative ( $-0.11$  V) for Ca-MnO<sub>x</sub>/Vulcan whilst for Ni-MnO<sub>x</sub>/Vulcan it was more positive ( $+0.06$  V). For the Mg-doped catalyst the potential was similar to the un-doped material (Fig. 4). Thus doping by Ni<sup>II</sup> (or possibly Mg<sup>II</sup>) may have facilitated decomposition of peroxides. In the case of MnO<sub>x</sub>/Monarch-based catalysts, doping by Ni was beneficial, since it significantly increased the ORR activity of the MnO<sub>x</sub>/Monarch-based catalysts. Indeed the MA were ca. 19 and 9 A g<sub>MnO<sub>2</sub></sub><sup>-1</sup> (at 0.00 V vs. SHE) for Ni-MnO<sub>x</sub>/Monarch and MnO<sub>x</sub>/Monarch, respectively, compared with 100 A g<sub>Pt</sub><sup>-1</sup> for 20 wt.% Pt/Vulcan XC72 (Table 1). The positive effect of nickel doping on the ORR, has also been reported in alkaline medium and was explained by the ability of transition metal atoms to exist in several valencies [11–13]. Thus the transition metals assist the charge transfer to oxygen, leading to increased electronic interactions with the stabilized Mn<sup>III</sup> produced from MnO<sub>2</sub> by proton insertion in the ORR potential range.

As a comparison of activity, Yu et al. [5] showed that iron phthalocyanine supported on Vulcan XC72 from E-Tek (FePcVC) exhibited, in 50 mM phosphate buffer medium at pH 7.0, ORR activity close to that of 20 wt.% Pt/Vulcan XC72. The open circuit potential of FePcVC was ca.  $+0.50$  V vs. SHE compared with  $+0.55$  V vs. SHE for the Pt catalyst. Thus based on the relative cost of the catalysts, MnO<sub>x</sub>/C materials are promising as non-platinised catalysts for the ORR at neutral pH: the cost of manganese is at least 100 times lower than platinum (in June 2008, according to the New York stock exchange, the cost of platinum was ca. 70 \$ g<sup>-1</sup>, a ton of ore containing 48% of Mn costing ca. 120 \$).

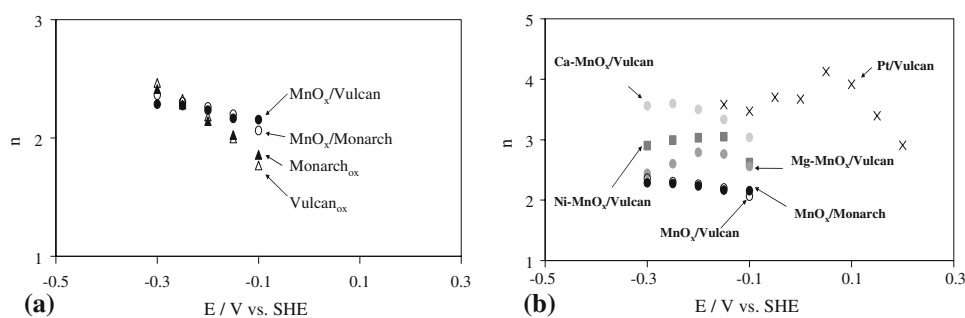
The stability of the MnO<sub>x</sub>/C-based catalysts was good as indicated by the reproducible LSVs in the ORR potential range. The first fuel cell tests using the carbon-supported manganese oxide ORR catalysts produced constant performance, suggesting no loss of active material. Long term (months) of fuel cell testing is needed to assess catalyst stability and will be reported later.

### 3.4 ORR mechanism

In alkaline solution, the ORR on MnO<sub>x</sub>/C involves two competitive pathways [21]: the 4-electron reduction yielding OH<sup>-</sup> ions and the 2-electron pathway yielding peroxide ions as intermediates. The number of electrons exchanged per molecule of oxygen reduced on the active layer ( $n$ ) can be determined, in the ORR potential range, from the Levich slope  $B = 0.1 n$  (see part 3.2). Values of  $n$  for the MnO<sub>x</sub>/C-based and Pt/Vulcan XC72 (E-Tek) catalysts and the carbon supports, obtained from the experimental Levich slopes (see the examples of MnO<sub>x</sub>/Monarch, Fig. 3c), in the ORR potential range at neutral pH, are shown in Fig. 5.

The ORR mechanism was difficult to determine at neutral pH due to resistive effects induced by the low concentration of hydroxide ions in the solution. However from the data,  $n$  was close to 2 for the carbon supports, in agreement with previous data for the ORR mechanism on carbon, i.e. a 2-electron reduction yielding peroxides [4]. In the low current density range ( $E > -0.2$  V vs. SHE), the value of  $n$  (between 2 to 3) for both carbon supports increased with the addition of MnO<sub>x</sub> (Fig. 5a): manganese oxides have previously been shown to effectively decompose peroxides [11]. It was likely that the main part of the 2-electron reduction pathway was due to the presence of carbon. In the low current density range the Tafel slopes, were ca.  $-0.134$  and  $-0.177$  V dec<sup>-1</sup> for MnO<sub>x</sub>/Vulcan and MnO<sub>x</sub>/Monarch, respectively (Table 1) indicating that the ORR mechanism can be modified by the substrate. This behaviour suggests that the two catalysts had different surface characteristics, as indicated by the limiting currents shown in Fig. 4b, due to functionalisation of the carbon surface, yielding different electronic interactions with O<sub>2</sub> during the ORR. The ORR mechanism on MnO<sub>x</sub>/C at neutral pH was different to that in strong alkaline solution, for which the Tafel slope was ca.  $-0.06$  V dec<sup>-1</sup> in the low current density range [13]. This suggests that at neutral pH more peroxide is formed per molecule of reduced oxygen in the ORR potential range.

**Fig. 5** Variation of number of electrons  $n$  with potential in the ORR potential range O<sub>2</sub>-saturated 0.1 M Na<sub>2</sub>SO<sub>4</sub> solution, 25 °C. (a) MnO<sub>x</sub>/Vulcan, MnO<sub>x</sub>/Monarch, Ni-MnO<sub>x</sub>/Monarch and the carbon supports, previously oxidised. (b) (MnO<sub>x</sub>/C-based catalysts and the benchmark 20 wt.% Pt/Vulcan XC72



The value of  $n$  increased with metal ion doping of the carbon-based manganese oxide catalysts (Fig. 5b) in agreement with observations in high pH (alkaline) medium [13]. This was more significant for the Ca-MnO<sub>x</sub>/Vulcan catalyst ( $n$  between 3 and 4) where doping orientated the ORR mechanism towards the 4-electron reduction pathway and produced fewer peroxide intermediates. Metal insertion increased the inter-plane distance between the manganese oxide layers (such as observed by XRD, see part 3.1) and the probability of water in the lattice and, as a consequence, the disproportionation of peroxides by MnOOH in aqueous medium, leading to an apparent 4-electron oxygen reduction. The presence of water in the MnO<sub>2</sub> lattice has been previously shown for carbon-supported manganese oxide nanoparticles [22]. In that context, calcium doping was more beneficial than nickel or magnesium doping (atomic distance of 180 pm for Ca compared with 150 and 135 pm for Mg and Ni, respectively). However, in the case of MnO<sub>x</sub>/Vulcan-based catalysts, the Tafel slope significantly changed with the Ni or Mg doping, whereas with Ca it did not (Table 1). The high values of  $b$ , ca.  $-0.335$  and  $-0.305$  V dec<sup>-1</sup> for Ni- and Mg-MnO<sub>x</sub>/Vulcan are, however, questionable as they indicate a very slow oxygen adsorption reaction and/or the blocking of such active layers by either a reaction intermediate (e.g. hydrogen peroxides) or adsorbed anions such as SO<sub>4</sub><sup>2-</sup>. Increasing electronic interactions, due to the presence of Ni (see part 3.2), may change the oxygen adsorption step on MnO<sub>x</sub>/C and lead to greater disproportionation of peroxides by MnOOH [21].

In the case of Monarch-supported manganese oxide nanoparticles, Ni doping did not dramatically change the Tafel slope in the low current density range; i.e.  $b$  was ca.  $-0.177$  V dec<sup>-1</sup> for MnO<sub>x</sub>/Monarch (cf.  $-0.113$  V dec<sup>-1</sup> for Ni-MnO<sub>x</sub>/Monarch). However, the value of  $n$  was ca. 4 for Ni-MnO<sub>x</sub>/Monarch, suggesting the 4-electron ORR mechanism was predominant. This is of great significance for fuel cells where peroxides can lead to corrosion of catalyst supports.

The determination of  $n$  from the Levich slopes is not very accurate, especially in the high current density range ( $E < -0.2$  V vs. SHE). Rotating ring disc electrode (RRDE) experiments are preferred to determine the percentage of peroxides formed per molecule of reduced oxygen. Overall the ORR mechanism on MnO<sub>x</sub>/C materials in neutral pH solution may proceed via two parallel pathways. These are direct 4-electron reduction of O<sub>2</sub> to OH<sup>-</sup>, which mainly occurs on manganese oxide particles, and a 2-electron reduction of O<sub>2</sub> yielding HO<sub>2</sub><sup>-</sup>, especially on the carbon support, peroxide ions then being decomposed either on the MnO<sub>x</sub>/C catalyst or in solution. The MnO<sub>2</sub>/MnOOH species may act as an oxygen mediator (acceptor/donor), with the first step of both pathways being proton

insertion (2). The divalent metals may facilitate decomposition of HO<sub>2</sub><sup>-</sup> on the metal-MnO<sub>x</sub>/C, the 4-electron pathway then being more apparent.

#### 4 Conclusions

The ORR on MnO<sub>x</sub>/C-based catalysts has been characterised in neutral pH solution using an RDE. These catalysts are promising as cathode materials for microbial fuel cells. The Mn<sup>III</sup>/Mn<sup>IV</sup> species can act as mediators in the oxygen reduction mechanism, similar to that proposed in alkaline medium. The doping of manganese oxides by divalent ions enhanced the ORR. The ORR mechanism on MnO<sub>x</sub>/C catalysts was either a 4-electron pathway or an indirect 2-electron pathway, yielding peroxides, followed by their decomposition. The metal doping of MnO<sub>x</sub> orientated the ORR mechanism towards the 4-electron pathway, yielding less peroxides as intermediates.

**Acknowledgments** This research was supported by the European Union through a Transfer of Knowledge award on biological fuel cells (contract MTKD-CT-2004-517215).

#### References

1. Gil GC, Chang IS, Kim BH, Kim M, Jang JK, Park HS, Kim HJ (2003) *Biosens Bioelectron* 18:327
2. Jang JK, Pham TH, Chang IS, Kang KH, Moon H, Cho KS, Kim BH (2004) *Process Biochem* 39:1007
3. Pham TH, Jang JK, Chang IS, Kim BH (2004) *J Microbiol Biotechnol* 14:324
4. Kinoshita K (1992) In: *Electrochemical oxygen technology*. Wiley, New York
5. Hao Yu E, Cheng S, Scott K, Logan B (2007) *J Power Sources* 171:275
6. Clauwaert P, Van der Ha D, Boon N, Verbeken K, Verhaege M, Rabaey K, Verstraete W (2007) *Environ Sci Technol* 41:7564
7. Nguyen Cong H, Chartier P, Brenet J (1977) *J Appl Electrochem* 7:383–395
8. Heller-Ling N, Poillierat G, Koenig JF, Gautier JL, Chartier P (1994) *Electrochim Acta* 39:1669
9. Calegari ML, Lima FHB, Ticianelli EA (2006) *J Power Sources* 158:735
10. Bezdička P, Grygar T, Klápště B, Vondrák J (1999) *Electrochim Acta* 45:913
11. Klápště B, Vondrák J, Velická J (2002) *Electrochim Acta* 47:2365
12. Vondrák J, Klápště B, Velická J, Sedlaříková M, Reiter J, Roche I, Chainet E, Fauvarque JF, Chatenet M (2005) *J New Mater Electrochem Syst* 8:209
13. Roche I, Chainet E, Chatenet M, Vondrák J (2007) *J Phys Chem C* 111:1434
14. Roche I (2007) Thèse de doctorat, INPG
15. Zhang XG, Shen CM, Li HL (2001) *Mater Res Bull* 36:541
16. Warren BE (1990) In: *X-ray diffraction*. Dover Publications, Dover, New York, p 251
17. Pourbaix M (1963) In: *Atlas d'équilibres électrochimiques*. Gauthier-Villard, Paris

18. Kozawa A, Yeager JF (1965) *J Electrochem Soc* 112:959
19. Diard JP, Le Gorrec B, Montella C (1996) In: *Cinétique Electrochimique*. Herman, Paris
20. Gloaguen F, Andolfatto D, Durand R, Ozil P (1994) *J Appl Electrochem* 24:863
21. Mao L, Zhang D, Sotomura T, Nakatsu K, Koshiha N, Ohsaka T (2003) *Electrochim Acta* 48:1015
22. Roche I, Chainet E, Chatenet M, Vondrák J (2008) *J Appl Electrochem* (in press)